Controlling Thermal Conductivity of Alloys via Atomic Ordering

John C. Duda[1]
e-mail: duda@virginia.edu

Timothy S. English

Donald A. Jordan

Pamela M. Norris

Department of Mechanical and Aerospace Engineering,
University of Virginia,
Charlottesville, VA 22904

William A. Soffa
Department of Materials Science and Engineering,
University of Virginia,
Charlottesville, VA 22904

Many random substitutional solid solutions (alloys) will display a tendency to atomically order given the appropriate kinetic and thermodynamic conditions. Such order–disorder transitions will result in major crystallographic reconfigurations, where the atomic basis, symmetry, and periodicity of the alloy change dramatically. Consequently, phonon behavior in these alloys will vary greatly depending on the type and degree of ordering achieved. To investigate these phenomena, the role of the order–disorder transition on phononic transport properties of Lennard–Jones type binary alloys is explored via nonequilibrium molecular dynamics simulations. Particular attention is paid to regimes in which the alloy is only partially ordered. It is shown that by varying the degree of ordering, the thermal conductivity of a binary alloy of fixed composition can be tuned across an order of magnitude at 10% of the melt temperature, and by a factor of three at 40% of the melt temperature. [DOI: 10.1115/1.4004843]

Keywords: thermal conductivity, molecular dynamics simulations, order–disorder transitions, alloys

1 Introduction

Substitutional solid solutions, or alloys, can exist in both *atomically* ordered and disordered states. While identical in terms of composition, these states are distinguished from each other by their unique crystallographic configurations. In the disordered state (random alloy), atoms are arranged in a statistically random distribution among the atomic sites of the crystalline lattice, where the probability of finding a particular type of atom at any given atomic site is based on the stoichiometry of the solution itself [1]. It is important to note that, in this context, disorder does not imply a deviation from crystallinity. In the ordered state, atoms are situated in a specific arrangement within each unit cell [2], and each type of atom is said to occupy its own sublattice [3].

The particular crystallographic configuration in which a system will order depends on several factors, e.g., the number and types of constituent atoms comprising the solution, as well as the stoichiometric ratio of the solution itself. The $L1_1$ configuration is one in which atoms arrange themselves such that a 1×1 superlattice forms along the [111] crystallographic direction relative to the conventional face-centered-cubic (fcc) lattice vectors from which this ordered phase is derived. CuPt is a classic example of a metallic system that can exhibit $L1_1$ ordering, where the ordered phase is achieved by annealing the corresponding disordered alloy at temperatures below the critical temperature [1,3]. Additionally, it has been shown that group IV binary [4–6] and group III-V ternary and quaternary [7,8] semiconductor alloys can exhibit analogous "$L1_1$-type" ordering. However, in semiconductor systems, long-range order can only be achieved through thin-film growth under very particular conditions [4–8].

In disordered fcc AB alloys, there is a 50-50 chance of finding either an A or a B atom at each atomic site of an fcc lattice (A1 Strukturbericht designation). In $L1_1$ ordered AB alloys, atoms preferentially arrange themselves such that there is an A atom at (0, 0, 0) and a B atom at (1, 1, 1), again with respect to the conventional lattice vectors of the A1 configuration. Despite the fact that both the A1 an $L1_1$ primitive cells are rhombohedral, the $L1_1$ primitive cell can only be formed along a single body diagonal of the conventional cell, indicating that the $L1_1$ configuration has only a single axis of three-fold (trigonal) symmetry as opposed to the four axes of three-fold symmetry of the A1 configuration.

As a result of this crystallographic reconfiguration, the properties of ordered and random alloys can differ greatly. Many theoretical, experimental, and computational studies have investigated changes in material properties across the order–disorder transition in both metallic and semiconductor systems. These include studies of electrical resistivity [9,10], electronic band gap and band structure [11,12], magnetic anisotropy [13], Raman spectra [6,14], and vibrational properties [15,16]. Despite these investigations, the role of the order–disorder transition on phononic thermal conductivity (κ) has been left largely unexplored [17].

In the present study, we have employed nonequilibrium molecular dynamics (NEMD) simulations to investigate the sensitivity of thermal conductivity (κ) to the degree of atomic ordering in AB Lennard–Jones (LJ) type binary alloys. Thermal fluxes are applied in the [001] crystallographic direction relative to the cubic conventional lattice of the corresponding A1 system, thus mimicking a situation in which a thermal flux would be applied in the "growth direction" of ordered SiGe thin films [4,5]. Special attention is given to the thermal conductivity of partially ordered alloys, thus establishing a gauge for future experimental validation. It is shown that by varying the degree of ordering, the thermal conductivity of a binary alloy of fixed composition can be tuned across an order of magnitude at 10% of the melt temperature, and by a factor of three at 40% of the melt temperature.

2 Molecular Dynamics Simulations

We have employed NEMD simulations to study κ of ordered, partially ordered, and disordered LJ binary alloys. Nonequilibrium molecular dynamics is a technique in which a heat flux is applied across a computational domain and a steady-state, one-dimensional temperature gradient is established. With the thermal flux and temperature gradient known, κ can be calculated via Fourier's law. This technique has been used extensively to investigate thermal transport properties in nanoscopic systems, e.g., thermal conductivity [18–21] and thermal boundary conductance [22–24]. While the LJ interatomic potential implemented in this study cannot exactly reproduce the properties of many materials beyond inert gases, such simulations are still able to produce physically meaningful results, especially in the context of phononic (vibrational) properties [20–23].

2.1 Computational Details. The A- and B-type atoms in the various domains were distinguished by their atomic masses, which were 40 and 120 atomic mass units, respectively. The LJ parameters for both the A and B atoms were fixed ($\varepsilon = 0.0503$ eV and $\sigma = 3.37$ Å). All results are presented in non-dimensional (reduced LJ) units

[1]Corresponding author.

Contributed by the Heat Transfer Division of ASME for publication in the JOURNAL OF HEAT TRANSFER. Manuscript received November 23, 2010; final manuscript received August 1, 2011; published online October 28, 2011. Assoc. Editor: Robert D. Tzou.

$$E^* = \frac{E}{\varepsilon}, \quad T^* = T\frac{k_B}{\varepsilon}, \quad \omega^* = \omega\sqrt{\frac{\sigma^2 m}{\varepsilon}}, \quad \kappa^* = \kappa\frac{m^{0.5}\sigma^2}{\varepsilon^{0.5}k_B} \tag{1}$$

where m is the mass of an A atom (40 amu), and E, T, and ω, are energy, temperature, and angular frequency, respectively. From this point forward, asterisks will be dropped and all discussion will make use of nondimensional units.

All eight computational domains implemented in this study were $31.6 \times 31.6 \times 232$ Å^3 and contained 6336 atoms. The four outermost layers of atoms in all domains formed a rigid wall to prevent sublimation from the free surface of the domain during nonequilibrium heating. The eight layers of atoms immediately inside these rigid walls were "bath" atoms, to which energy was added or removed during nonequilibrium heating. The remaining atoms are "normal atoms" such that they do not have any external conditions imposed on them. The domains differed from each other by way of their respective Bragg-Williams long-range order parameter, $\eta = (R - W)/(R + W)$, where R and W refer to the number of atoms that are in the "right" and "wrong" positions in the context of the perfectly ordered crystal. Order parameters implemented in this study were 1, 0.99, 0.95, 0.90, 0.85, 0.75, 0.50, and 0. Schematics of selected computational cells ($\eta = 1$, 0.75, and 0) are shown in Fig. 1.

During the simulation, the equations of motion for the system were integrated using the Nordsieck fifth-order predictor corrector algorithm [25]. Periodic boundary conditions were initially applied in all directions, and the system was equilibrated at a predefined temperature via a velocity scaling routine ($0.046 \leq T \leq 0.470$, depending on the simulation) and zero pressure. Zero pressure was maintained by the Berendsen barostat algorithm [26]. Once equilibration was complete, the periodic boundary conditions in the z-direction were switched to free boundary conditions, and the nonequilibrium heating procedure was implemented. The addition/removal of energy to/from the baths was performed through a constant energy approach, allowing for thermal flux across the computational cell to be controlled explicitly. This routine slightly changes the forces acting on an atom depending on the amount of energy to be added or removed [27]. To ensure the baths were not being perturbed far from equilibrium they were sized such that the amount of energy added to or removed from the bath was less than 1% of the bath kinetic energy.

During nonequilibrium heating, the system was divided into 40 equally sized slices such that a spatial-temperature profile could be calculated along the z-axis. The temperature of each of these slices, T_S, was determined through the relationship

$$\frac{3}{2}N_S k_B T_S = \sum_{i=1}^{N_S}\frac{1}{2}m_i(v_i^T)^2 \tag{2}$$

where N_S is the number of atoms in a particular slice S, and k_B is the Boltzmann constant. Each slice was comprised of approximately 160 atoms. Linear fits of T_S versus time data were made for discrete time intervals during the simulation, and the slopes of these lines were used to determine the onset of the steady-state regime. Once in the steady-state regime, time-averaged spatial-temperature profiles were created. To determine the temperature gradient, a linear least squares fit was performed for each temperature profile. The slices (roughly two atomic layers) nearest to the baths were not included in the fits. From the spatial-temperature profiles, and with the applied flux known, κ of the alloys were calculated via Fourier's law. The applied fluxes were chosen such that the temperature drop across the domain did not exceed 15% of the average domain temperature. However, this limit was only realized for the lower-temperature simulations. In reality, the temperature drop for the majority of the simulations was closer to 5% of the average domain temperature.

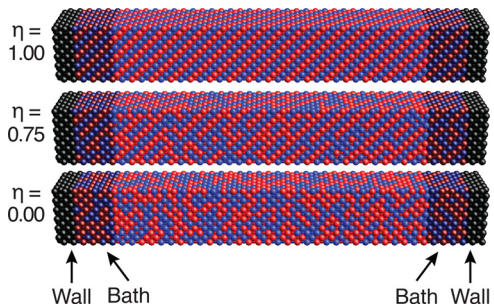

Fig. 1 Selected computational domains

2.2 Density of States Calculations. Phonon density of states (DOS) curves of the eight computational domains was calculated. The DOS is defined as the Fourier transform of the velocity autocorrelation function [23,28] but, in practice, is calculated using standard estimation procedures for power spectral density. For each atom, the velocity is obtained at each time step to give a velocity fluctuation time series of 36,864 points. The Welch method of power spectral density estimation is then applied by creating eight 50% overlapping segments of 8192 points. Each segment is then multiplied by a Hamming window, and the fast Fourier transform is computed. The DOS is then obtained by ensemble averaging the Fourier transform magnitudes of each segment.

The DOS curves of three selected alloys are shown in Fig. 2. As is evident from the plot, all domains have nearly identical vibrational spectra in the low- and high-frequency limits. In the low-frequency limit, phonons do not observe the discreteness of the crystal and continuum theory applies. Since all domains have the same average mass density and the same elastic constants, long wavelength phonons effectively "see" the same effective continuum in each of the domains, regardless of order parameter. In the high-frequency limit, this behavior can be explained by the fact that the highest-frequency vibrational modes will be those between two A atoms. That is, since the effective spring constant between all atoms is the same and $\omega \propto \sqrt{K/(m_1 m_2)^{0.5}}$, the maximum frequency is related to the vibrations between groups of the lightest atoms.

Apart from these limits, it is clear from these plots that the distribution of vibrational modes changes between these two limits as the alloys become more ordered. In particular, the development of vibrational peaks at $\omega = 7$ and 19, as well as the trough between them, is apparent. As the order-parameter increases, the domain approaches the limit in which a 1×1 superlattice appears along the [111] crystallographic direction. It has been shown that in short-period superlattices, phonon interference leads to the formation of "optical" type phonon branches and, in turn, the formation of phononic band gaps or stop bands [20]. This behavior manifests

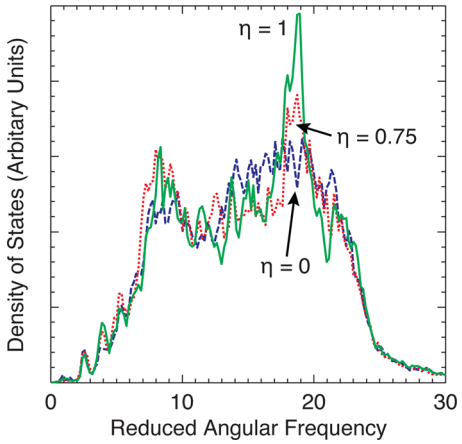

Fig. 2 Phonon density of states curves

itself in the DOS curves through the formation of the respective peaks and troughs described above. However, a full band gap is not realized, as the DOS curve represents the vibrational summary of the entire Brillouin zone, not just that in the direction perpendicular to the superlattice. It is also important to note that substantial long-range ordering must be achieved to see significant changes in the DOS curves, suggesting the same may be true in terms of changes in κ as well.

2.3 Thermal Conductivity Predictions. Thermal conductivity predictions for the eight order parameters considered are shown as functions of temperature in Fig. 3. Each individual point represents the average value calculated from five independent simulations, and error bars represent the standard deviation of these values, i.e., repeatability. The dependence of thermal conductivity on temperature in the limits of complete order and disorder is indicative of the specific phonon scattering mechanisms that dominate thermal conductivity in these domains. In the limit of absolute order ($\eta = 1$), thermal conductivity is inversely proportional to temperature, suggesting that the dominant phonon scattering mechanism is the Umklapp three-phonon scattering event [29]. In the limit of complete disorder ($\eta = 0$), thermal conductivity is only very weakly a function of temperature and is ultimately limited due to scattering of phonons by mass fluctuations, i.e., impurity scattering [30].

It is also interesting that the thermal conductivities of all domains begin to converge at elevated temperatures. In reality, the absolute convergence point is not directly observed as the crystals melt before this temperature is achieved ($T_{\text{melt}} \approx 0.5$ [23]). This convergence phenomenon can be explained in the following way. Thermal conductivity can be expressed as $\kappa = 1/3 c_v v^2 \tau$, where c_v is the volumetric heat capacity, v is the phonon group velocity, and τ is the total scattering time. Heat capacity of all domains will be the same ($c_v = 3Nk_B\rho$, where ρ is molar density) regardless of the degree of ordering, suggesting differences in κ are the result of differences in the $v^2\tau$ product. At high temperatures, the rate of Umklapp scattering ($\tau_U \propto T^{-1}$) in the ordered alloys "catches up" to the rate of impurity scattering in the random alloys, leading to the observed convergence of κ.

Lastly, it is clear that at low to moderate temperatures ($0 > T > 0.25$, or up to $\approx 0.5\ T_{\text{melt}}$) κ is very strongly dependent on η. In addition, it appears the strongest sensitivity to η is in the regime where η is approaches unity. For example, at $T = 0.133$, κ decreases by 48% when η goes from 1 to 0.9, whereas it only decreases 31% when η goes from 0.9 to 0.75. This behavior is consistent with that observed in dilute $Si_{1-x}Ge_x$ alloys, where the effect of the inclusion of more Ge "impurities" on κ becomes less pronounced with increasing Ge concentration [31]. The concentration of impurities, in this case, is analogous to the number of wrong atoms in the crystal, W, described above in the context of the ordering parameter. This nonmonotonic behavior is consistent with the observed trends in the DOS curves discussed above.

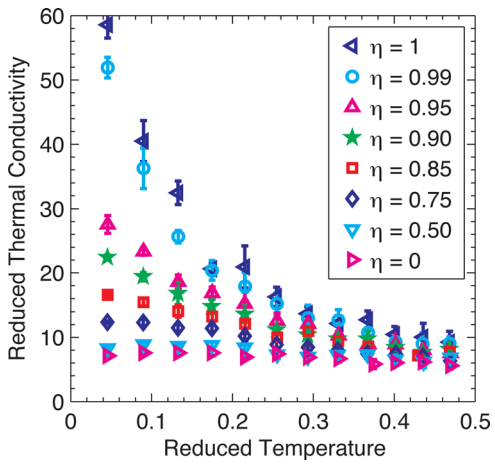

Fig. 3 Thermal conductivity predictions via NEMD

In order to ensure the above results were not affected by the limited size of the computational domain, a second computational domain at $\eta = 1$ was created 50% larger than that reported above. Thermal conductivity predictions of this larger domain were within the standard deviation of the predicted values of the smaller domain, suggesting the eight domains described above were large enough to capture the largest bulk phonon mean-free-paths that contribute to κ.

3 Conclusions

The role of atomic order on thermal conductivity of binary alloys has been examined via nonequilibrium molecular dynamics simulations. It has been shown that the thermal conductivity of a binary alloy of fixed composition can be tuned across an order of magnitude at 10% of the melt temperature and by a factor of three at 40% of the melt temperature so long as relatively high order parameters can be achieved (>75%). Additionally, the thermal conductivity of all alloys converges at high temperatures regardless of the order parameter. This behavior is attributed to the convergence of the respective $v^2\tau$ product (group velocity squared times phonon scattering time) in the ordered and disordered states. Again, since the observed effect is largest at low temperatures, atomic ordering could serve as a viable means of tuning the thermal conductivity of semiconductor alloys in low temperature applications.

Acknowledgment

The authors acknowledge the financial support of the Air Force Office of Scientific Research (Grant No. FA9550-09-1-0245). J.C.D. and T.S.E. are appreciative of support from the National Science Foundation through the Graduate Research Fellowship Program.

References

[1] Barrett, C. S., and Massalski, T. B., 1966, *Structure of Metals*, 3rd ed., McGraw-Hill, New York.
[2] Callister, W. D., and Rethwisch, D. G., 2010, *Materials Science and Engineering: An Introduction*, 8th ed., John Wiley & Sons, Hoboken, NJ.
[3] Sato, H., 1970, "Order-Disorder Transformations," *Solid-State* (Physical Chemistry: An Advanced Treatise, Vol. 10), W. Jost, ed., Academic, New York, Chap. 10.
[4] LeGoues, F. K., Kesan, V. P., Iyer, S. S., Tersoff, J., and Tromp, R., 1990, "Surface-Stress-Induced Order in SiGe Alloy Films," Phys. Rev. Lett., **64**(17), pp. 2038–2041.
[5] LeGoues, F. K., Kesan, V. P., and Iyer, S. S., 1990, "Long-Range Order in Thick, Unstrained $Si_{0.5}Ge_{0.5}$ Epitaxial Layers," Phys. Rev. Lett., **64**(1), pp. 40–43.
[6] Tsang, J. C., Kesan, V. P., Freeouf, J. L., LeGoues, F. K., and Iyer, S. S., 1992, "Raman Spectroscopy of Long-Range Order in Epitaxial $Si_{0.5}Ge_{0.5}$ Alloys," Phys. Rev. B, **46**(11), pp. 6907–6914.
[7] Jen, H. R., Cao, D. S., and Stringfellow, G. B., 1989, "Long-Range [111] Ordering in $GaAs_{1-x}P_x$," Appl. Phys. Lett., **54**(19), pp. 1890–1892.
[8] Shahid, M. A., Mahajan, S., Laughlin, D. E., and Cox, H. M., 1987, "Atomic Ordering in $Ga_{0.47}In_{0.53}As$ and $Ga_xIn_{1-x}As_yP_{1-y}$ Alloy Semiconductors," Phys. Rev. Lett., **58**(24), pp. 2567–2570.
[9] Ho, C. Y., Ackerman, M. W., Wu, K. Y., Havill, T. N., Bogaard, R. H., Matula, R. A., Oh, S. G., and James, H. M., 1983, "Electrical Resistivity of Ten Selected Binary Alloy Systems," J. Phys. Chem. Ref. Data, **12**(2), pp. 183–322.
[10] Fink, V., Chevalier, E., Pitts, O. J., Dvorak, M. W., Kavanagh, K. L., Bolognesi, C. R., Watkins, S. P., Hummel, S., and Moll, N., 2001, "Anisotropic Resistivity Correlated With Atomic Ordering in p-Type GaAsSb," Appl. Phys. Lett., **79**(15), pp. 2384–2386.
[11] Suzuki, T., Gomyo, A., Iijima, S., Kobayashi, K., Kawata, S., Hino, I., and Yuasa, T., 1988, "Band-Gap Energy Anomaly and Sublattice Ordering in GaInP and AlGaInP Grown by Metalorganic Vapor Phase Epitaxy," Jpn. J. Appl. Phys., **27**, pp. 2098–2106.
[12] Zunger, A., 1997, "Spontaneous Atomic Ordering in Semiconductor Alloys: Causes, Carriers, and Consequences," MRS Bull., pp. 20–26.
[13] Christodoulides, J., Farber, P., Dannl, M., Okumura, H., Hadjipanaysi, G., Skumryev, V., Simopoulos, A., and Weller, D., 2001, "Magnetic, Structural and Microstructural Properties of FePt/M (M = C,BN) Granular Films," IEEE Trans. Magn., **37**(4), pp. 1292–1294.

[14] Cheong, H. M., Mascarenhas, A., Ernst, P., and Geng, C., 1997, "Effects of Spontaneous Ordering on Raman Spectra of $GaInP_2$," Phys. Rev. B, **56**(4), pp. 1882–1887.
[15] Ozoliņš, V., and Zunger, A., 1998, "First-Principles Theory of the Evolution of Vibrational Properties With Long-Range Order in $GaInP_2$," Phys. Rev. B, **57**(16), pp. R9404–R9407.
[16] Fultz, B., 2010, "Vibrational Thermodynamics of Materials," Prog. Mater. Sci., **55**(4), pp. 247–352.
[17] Duda, J. C., English, T. S., Jordan, D. A., Norris, P. M., and Soffa, W. A., 2011, "Reducing Thermal Conductivity of Binary Alloys Below the Alloy Limit via Chemical Ordering," J. Phys.: Condens. Matter, **23**, p. 205401.
[18] Lukes, J. R., Li, D. Y., Liang, X.-G., and Tien, C.-L., 2000, "Molecular Dynamics Study of Solid Thin-Film Thermal Conductivity," ASME J. Heat Transfer, **122**, pp. 536–543.
[19] Abramson, A. R., Tien, C.-L., and Majumdar, A., 2002, "Interface and Strain Effects on the Thermal Conductivity of Heterostructures: A Molecular Dynamics Study," ASME J. Heat Transfer, **124**(5), pp. 963–970.
[20] McGaughey, A. J. H., Hussein, M. I., Landry, E. S., Kaviany, M., and Hulbert, G. M., 2006, "Phonon Band Structure and Thermal Transport Correlation in a Layered Diatomic Crystal," Phys. Rev. B, **74**(10), p. 104304.
[21] Landry, E. S., Hussein, M. I., and McGaughey, A. J. H., 2008, "Complex Superlattice Unit Cell Designs for Reduced Thermal Conductivity," Phys. Rev. B, **77**(18), p.184302.
[22] Twu, C.-J., and Ho, J.-R., 2003, "Molecular-Dynamics Study of Energy Flow and the Kapitza Conductance Across an Interface With Imperfection Formed by Two Dielectric Thin Films," Phys. Rev. B, **67**, p. 205422.
[23] Stevens, R. J., Zhigilei, L. V., and Norris, P. M., 2007, "Effects of Temperature and Disorder on Thermal Boundary Conductance at Solid-Solid Interfaces: Nonequilibrium Molecular Dynamics Simulations," Int. J. Heat Mass Transfer, **50**, pp. 3977–3989.
[24] Landry, E. S., and McGaughey, A. J. H., 2009, "Thermal Boundary Resistance Predictions From Molecular Dynamics Simulations and Theoretical Calculations," Phys. Rev. B, **80**(16), p. 165304.
[25] Allen, M. P., and Tildesley, D. J., 1990, *Computer Simulation of Liquids,* Clarendon, Oxford.
[26] Berendsen, H. J. C., Postma, J. P. M., van Gunsteren, W. F., DiNola, A., and Haak, J. R., 1984, "Molecular Dynamics With Coupling to an External Bath," J. Chem. Phys., **81**(8), pp. 3684–3690.
[27] Ivanov, D. S., and Zhigilei, L. V., 2003, "Combined Atomistic-Continuum Modeling of Short-Pulse Laser Melting and Disintegration," Phys. Rev. B, **68**, p. 064114.
[28] Zhigilei, L. V., Srivastava, D., and Garrison, B. J., 1997, "Vibrational Dynamics of the CH Stretching Mode of H-Terminated Diamond Surfaces," Surf. Sci., **374**(1–3), pp. 333–344.
[29] Chen, G., 2005, *Nanoscale Energy Transport and Conversion: A Parallel Treatment of Electrons, Molecules, Phonons, and Photons*, Oxford University Press, New York.
[30] Abeles, B., 1963, "Lattice Thermal Conductivity of Disordered Semiconductor Alloys at High Temperatures," Phys. Rev., **131**(5), pp. 1906–1911.
[31] Cahill, D. G., Watanabe, F., Rockett, A., and Vining, C. B., 2005, "Thermal Conductivity of Epitaxial Layers of Dilute SiGe Alloys," Phys. Rev. B, **71**(23), p. 235202.